J Appl Electrochem (2013) 43:331–345
DOI 10.1007/s10800-012-0508-z

ORIGINAL PAPER

Hydroxyapatite coating on selectively passivated and sensitively polymer-protected surgical grade stainless steel

D. Gopi · J. Indira · L. Kavitha · J. M. F. Ferreira

Received: 20 August 2012 / Accepted: 12 November 2012 / Published online: 29 November 2012

Abstract Surgical grade stainless steel (316L SS) is a widely used implant material in orthopedic surgeries. However, the release of metallic ions evidenced from the 316L SS implants in vivo conditions is a big challenge. In order to minimize the release of metallic ions, coating the 316L SS implant with a biocompatible material like hydroxyapatite [HAP, $Ca_{10}(PO_4)_6(OH)_2$] is one of the suitable methods. In this paper, the hydroxyapatite coating on borate passivated through poly-*ortho*-phenylenediamine (PoPD)-coated 316L SS by a dip coating method has been reported. The coatings were characterized by electrochemical techniques such as potentiodynamic polarization, electrochemical impedance spectroscopy, and cyclic voltammetry. Surface characterization studies of the coatings such as X-ray diffraction (XRD), X-ray photoelectron spectroscopy (XPS), and scanning electron microscopy (SEM) were also carried out. The leach out characteristics of the coatings was determined at the impressed potential. The mechanical property of the coatings was evaluated by Vicker's microhardness test. The Cr-rich passive film formed underneath the PoPD layer showed a higher protective efficiency. The ability to form apatite on the post-passivated PoPD-coated 316L SS specimen was examined by immersing it in the simulated body fluid. The enhanced corrosion resistivity of the HAP coating on the post-passivated PoPD-coated 316L SS was due to an effective barrier of PoPD followed by the passive film underneath the PoPD.

Keywords 316L SS · Hydroxyapatite coating · Passive film · Conductive polymer · Electrochemical impedance spectroscopy

1 Introduction

For the past few decades, surgical grade stainless steel (316L SS) (ASTM F138), Co-based alloys and titanium alloys have been the most commonly used surgical grade implant materials in dental and orthopedic fields due to their good biocompatibility, excellent mechanical properties, and high corrosion resistance. The need to reduce costs in public health services has compelled the use of SS as the most economical alternative for orthopedic implants [1–4]. However, the SS was unable to withstand the physiological environments over long period of time and can lead to the release of metallic ions such as Ni^{2+}, Cr^{3+}, and Cr^{6+} causing local systemic effects, and thereby play a role in prosthetic loosening that could finally end in the removal of the implant [5–9]. Therefore, decreasing the release of metallic ions is highly essential to avoid the deleterious effects caused by the corrosion products in normal bone formation. Hydroxyapatite, the biocompatible ceramic is used as a coating material

D. Gopi (✉) · J. Indira
Department of Chemistry, Periyar University, Salem 636 011, Tamil Nadu, India
e-mail: dhanaraj_gopi@yahoo.com

D. Gopi · L. Kavitha
Centre for Nanoscience and Nanotechnology, Periyar University, Salem 636 011, Tamil Nadu, India
e-mail: louiskavitha@yahoo.co.in

L. Kavitha
Department of Physics, Periyar University, Salem 636 011, Tamil Nadu, India

L. Kavitha
The Abdus Salam International Centre for Theoretical Physics, Trieste, Italy

J. M. F. Ferreira
Department of Ceramics and Glass Engineering, University of Aveiro, CICECO, 3810-193 Aveiro, Portugal

on the metallic substrates to resist the metal ion release and interact with the new tissue formation [10, 11].

However, due to the continuous interaction with the harsh environment, the HAP coating on the metallic surface degrades as time progresses, resulting in the corrosion of the underlying metallic alloy. Hence, the above reasons justify the surface treatment of 316L SS prior to deposit a HAP coating for preventing the metallic corrosion and withstanding the long-term implant conditions. Surface treatment procedures such as passivation [12, 13], electropolishing [14], and low temperature nitridization [15] have been used to enhance the resistivity of the metals. In this context, the present paper deals with a surface treatment of 316L SS substrate with a multilayer coating to prevent leaching out of the metal constituents effectively. SSs form passive film which provides the key to their high resistance to corrosive attack. It is a common agreement that an increased chromium-to-iron ratio in the surface passive film results in an increased resistance to pitting corrosion [16–18]. Our recent study proved that the passive film formed on SS from borate buffer solution under potentiostatic condition exhibited duplex character with an inner chromium oxide part along with an outer iron oxide part and these films have greatest corrosion resistance [19]. Recently, conductive polymers (CPs) are revealed to be promising materials for analytical applications [20]. It is already reported that PoPD has an excellent biocompatibility, permselectivity, and interference rejection behavior from oxidizable species [21]. Due to these characteristics, PoPD is used in the development of biosensors for in vivo neurochemical monitoring in brain as well as in estimating the glucose level in blood [20–28]. PoPD is also used for the corrosion protection of 304 SS and 430 SS types [29, 30]. Since no such work has been employed until now on the widely used 316L SS for biomedical applications, we have attempted the electrochemical selective passivation of PoPD-coated 316L SS from borate buffer solution at 0.64 V under potentiostatic condition. The efficiency of PoPD in making the chromium-enriched passive film on 316L SS by borate passivation and the effective protection of the passive film by PoPD coating are discussed. Moreover, the surface and electrochemical studies of HAP coating on borate passivated through PoPD-coated 316L SS surface is also carried out to investigate the corrosion resistivity and the stability of the coatings in Ringer's solution.

2 Experimental procedures

2.1 Preparation of alloy specimen

For our study, we have used 316L SS as working electrode. The elemental composition of 316L SS is (wt%) C 0.0222, Si 0.551, Mn 1.67, P 0.023, S 0.0045, Cr 17.05, Ni 11.65, Mo 2.53, Co 0.136, Cu 0.231, Ti 0.0052, V 0.0783, N 0.0659, and the rest Fe. The substrates are embedded in epoxy resin with a working area of 1 cm^2. The surface of the electrodes was abraded with different grades of SiC papers from 400 to 1,200 grit. The final polishing was done with coarse (6 μm) and fine (1 μm) diamond pastes in order to produce scratch-free mirror finish surface, and then degreased with acetone. This was followed by ultrasonic cleaning in acetone for 10 min and then the specimens were rinsed with deionized water, dried, and used for further studies.

2.2 Electrodeposition of PoPD on 316L SS

The electrodeposition process was carried out in three electrode cell assembly. The working electrode was type 316L SS. The counter and reference electrodes were platinum and saturated calomel electrode (SCE), respectively. The PoPD was electrodeposited on 316L SS by cyclic voltammetry (CV) between −0.5 and 1.2 V from 0.1 M H_2SO_4 solution (pH 1.0) containing 0.05 M *o*-phenylenediamine with a scan rate of 50 mV s^{-1} [29, 30]. All the potential in text are related to SCE. In order to study the corrosion resistance of the PoPD coating, the electrodeposition was carried out at three different voltammetric cycles such as 15, 30, and 50.

2.3 Post- and pre-passivation of PoPD-coated SS

Due to the excellent permselective nature of PoPD, the passive film beneath the PoPD layer was achieved by holding the PoPD-coated SS specimen under the potentiostatic condition at a potential of 0.64 V for 1 h in borate buffer solution (0.4 M of sodium tetraborate) with a pH of 9.3 [19]. After the electrochemical preparation, the specimens were rinsed with deionized water and dried for further coating. In order to compare, the pre-passivation of SS was achieved in borate buffer solution at 0.64 V followed by the PoPD coating.

2.4 Development of HAP coating

The suspension for dip coating of HAP was prepared by ultrasonic agitation of HAP powder synthesized from amino acid freezing method [31] in isopropyl alcohol. The HAP powder concentration in the suspension was 30 g L^{-1}. In this study, a computer controlled dip coater was employed to dip coat the pristine 316L SS specimen into the HAP suspension. The apparatus is provided with a two-way electronic switch in a provision to descend and ascend the substrates. The dipping of the suspension was maintained at a constant speed of 2,500 rpm with 5 mm min^{-1}. HAP coating on surface-treated SS specimens were done as before for

pristine 316L SS. Then the samples removed from the suspension were rinsed with distilled water and air-dried.

2.5 In vitro test in simulated body fluids

The biocompatibility of the post-passivated PoPD-coated 316L SS specimen is assessed in terms of its ability to form bone-like apatite layer over the surface when it is immersed in simulated body fluid (SBF). The SBF was prepared according to Kokubo's protocol [32], with concentration of ions nearly equal to those of the human blood plasma, as shown in Table 1. The SBF was prepared in deionized water by dissolving the reagents one by one from 1st to 8th in the order given in Table 2, and the temperature was maintained at 36.5 ± 1.5 °C. The pH of the solution was adjusted to 7.40 with 1 M HCl and tris-hydroxymethyl aminomethane (Tris) and finally the temperature was set to 36.5 °C. The post-passivated PoPD-coated specimen was soaked in SBF for different periods such as 7, 14, and 21 days. After soaking, the specimens were removed from SBF, washed with distilled water, acetone, and dried at room temperature. The SBF was renewed every day in order to preserve the ions concentration.

2.6 Characterization of the coating

2.6.1 Electrochemical characterization techniques

Electrochemical studies involving potentiodynamic anodic polarization and electrochemical impedance spectroscopy (EIS) were performed in Ringer's solution (NaCl 8.6 g L^{-1}, $CaCl_2{\cdot}2H_2O$ 0.66 g L^{-1}, and KCl 0.6 g L^{-1}) to assess the corrosion resistance due to surface treatment as well as HAP coating on surface-treated specimens. For electrochemical measurements, a CHI 760 electrochemical workstation (USA) was used. The working and counter electrodes were 316L SS and platinum, respectively. Also, the SCE was used as the reference electrode. All the potential values in the text are related to the SCE. The polarization study was carried out by increasing the potential in noble direction at a scan rate of 0.1 mV s^{-1} until the breakdown potential (E_b) is reached, and the sweep direction was reversed till the scan meets the passive region. The potential at which there was a monotonic increase in the current density is termed as breakdown potential or pitting potential (E_b). The potential at which the reverse scan meets the passive region is termed as the repassivation potential (E_p).

The electrochemical impedance studies were carried out in the same setup as that of potentiodynamic polarization studies, and the applied ac perturbation signal was about 0.01 V within the frequency range of 1 Hz to 100 kHz. All the impedance measurements were carried out at an open circuit potential (OCP). The CV studies were performed in borate buffer solution in the conventional way by running the potential between the cathodic and anodic limit from −1.0 to +1.0 V at a scan rate of 100 mV s^{-1} for detecting the presence of passive film at the substrate and the PoPD interface. In order to check the reproducibility of the results, at least three measurements were conducted for each specimen.

2.7 Surface characterization techniques

The presence of the passive film in the surface-treated specimens was studied by X-ray diffraction (XRD) using Bruker D8 Advance diffractometer, Germany. For the post-passivated PoPD-coated specimen, the passive film underneath the PoPD layer was investigated after scratching of the PoPD layer from SS surface and then washed with distilled water. The formation of passive film on the surface-treated 316L SS specimens were assessed by XPS, and it was performed with VG ESCA LAB Mark II spectrometer using an AlKα X-ray source with a mean kinetic energy of 1486.6 eV and a hemispherical electron analyzer operating at constant transmission-pass energy of 20 eV. The experiment was carried out at a vacuum of 10^{-7}–10^{-9} torr. The survey spectra were collected using Eclipse V 2.1 data-analysis software supplied by the manufacturer. The output of the photoelectron analysis was obtained as binding energy versus intensity counts. The binding energy scale was calibrated with respect to the C1s (284.5 eV). The evaluation of the survey spectra was performed using the parameters of standard peaks. To confirm the formation of calcium phosphate apatite layer on the surface of the post-passivated PoPD-coated 316L SS, Fourier transform infrared spectra were recorded using Nicolet 380 FT-IR spectrophotometer over the range from 4,000–400 cm^{-1} with a number of scans (32) and of resolution as 4 cm^{-1}. For this, small amount of as-formed apatite on the surface-treated alloy was scrapped, blended with KBr, and then pressed into discs for the measurement.

The surface morphology of uncoated, surface-treated, and surface-treated HAP-coated 316L SS specimens were studied by scanning electron microscope (SEM, JSM 840A Scanning microscope, JEOL Japan). To confirm the interfacial interaction of HAP coating on the post-passivated

Table 1 Ionic composition of human blood plasma and SBF [31]

Ions	Na^+	K^+	Ca^{2+}	Mg^{2+}	Cl^-	HCO_3^-	HPO_4^{2-}	SO_4^{2-}
Human blood plasma (mM)	142	5	2.5	1.5	103	27	1	0.5
SBF (mM)	142	5	2.5	1.5	147.8	4.2	1	0.5

Table 2 Reagents and their amounts used for preparing SBF [31]

S. no.	Reagents	Amount (g L^{-1})	Formula weight
1	NaCl	8.035	58.4430
2	$NaHCO_3$	0.355	84.0068
3	KCl	0.225	74.5515
4	$K_2HPO_4{\cdot}3H_2O$	0.231	228.2220
5	$MgCl_2{\cdot}6H_2O$	0.311	203.3034
6	1 M HCl	39 mL	36.5
7	$CaCl_2$	0.292	110.9848
8	Na_2SO_4	0.072	142.0428
9	Tris	6.118	121.14
10	1 M HCl	0–5 mL	36.5

PoPD-coated 316L SS, SEM cross-sectional view was carried out. The surface morphological changes that occurred on the post-passivated PoPD-coated 316L SS after the immersion in SBF were also scanned by SEM. The leach out characteristics of the coatings were determined by applying an impressed potential of 0.46 V (just above the breakdown potential (E_b) of pristine 316L SS) for specified duration of time (1 h) in Ringer's solution. At the end of the experiment the chemical composition of the test solution was analyzed. The analysis was carried out using inductively coupled plasma-atomic emission spectroscopy (ICP-AES; model: Thermo Electron IRIS INTREPID II XSP DUO) using Thermo Jarrel Ash-Atom Scan (USA).

2.8 Statistical analysis

The leach out of metal ions from untreated, surface-treated, and HAP coatings on surface-treated 316L SS were reported as mean ± standard deviation. The statistical differences were analyzed using one-way analysis of variance (ANOVA) followed by the student–Newman–Keuls post-hoc test, and the differences of $P < 0.05$ were considered to be statistically significant.

2.9 Adhesion test

The adhesion strength of the HAP-coated 316L SS and HAP coated on the post-passivated PoPD-coated 316L SS samples were assessed by pull-out test according to American Society for Testing Materials (ASTM) International Standard F1044. The coated 316L SS cylindrical specimens (25 mm in diameter by 25 mm in height) were bonded to uncoated cylinders surface with epoxy adhesive. The test specimens were cured at 100 °C for 60 min, and the pull-out test performed at a crosshead speed of 1 mm min^{-1}, using a universal testing machine (Model 5569, Instron). Five tests ($n = 5$) of adhesion strength were conducted for the same type of coating in order to obtain the average value of bonding strength. The adhesive strength of the coating was expressed by the unit mega Pascals (MPa).

2.10 Hardness test

Hardness test was performed on PoPD coated, the post-passivated PoPD-coated 316L SS, and HAP coated on the post-passivated PoPD-coated 316L SS specimens using Akashi AAV-500 series hardness tester. The load used was 490.3 mN and the load time was 20 s. Each hardness value is the average of 10 readings.

3 Results and discussion

3.1 Electrochemical characterization

3.1.1 Potentiodynamic cyclic anodic polarization

Polarization studies are the standard acceleration corrosion testing method in assessing the long-term "in vitro" corrosion behavior of metallic implants. The polarization curves recorded for the pristine- and surface-treated 316L SS specimens are shown in Fig. 1 and the corresponding E_b and E_p values are presented in Table 3. A close inspection on the polarization curves obtained reveals that the breakdown potential (E_b) and repassivation potential (E_p) values for pristine 316L SS were found to be 0.453 and 0.094 V, respectively. The PoPD-coated 316L SS specimen at two different voltammetric cycles such as 15, 30, showed E_b values of 0.488 and 0.541 V (SCE) (not shown in Fig. 1). While the E_b and E_p values recorded for the PoPD coating done at 50 cycles were 0.615 and 0.115 V, respectively. Thus, the E_b values obtained for PoPD-coated 316L SS were found to be nobler when compared with the uncoated 316L SS. Therefore, the PoPD coating done at 50 cycles was fixed as an optimum and taken for further studies because of its high E_b value. Furthermore, the polarization curve for the post-passivated PoPD-coated 316L SS showed higher E_b and E_p values, 0.683 V and 0.167 V, respectively, when compared to the PoPD-coated SS surface. Hence, the higher E_b and E_p values for such passivation through the PoPD coating confirms an appreciable increase in bio resistivity of coating, which is attributed to the formation of a passive film underneath the PoPD layer due to an excellent permselectivity of the PoPD.

It is also evident from Fig. 1 that the passive film formed electrochemically underneath the PoPD layer by a post-passivation of the PoPD-coated 316L SS offers a higher corrosion resistance than the film formed on the

pre-passivated PoPD-coated 316L SS, whose E_b and E_p values are found to be 0.620 and 0.155 V, respectively.

The enhanced corrosion resistance of the passive film is attributed to the selective dissolution of iron and enrichment of chromium ion in the passive film by PoPD. This finding was further substantiated by leach out study from pre-passivated PoPD-coated 316L SS, whose E_b and E_p values are found to be 0.620 and 0.155 V, respectively.

Figure 2 shows the polarization curves for HAP coated on untreated and surface-treated 316L SS specimens and the corresponding E_b and E_p values are presented in Table 3. The E_b and E_p values for HAP coated on pristine 316L SS specimen were found to be 0.488 and 0.103 V, respectively. From the polarization curves, it is demonstrated that the E_b and E_p values for HAP coated on the PoPD-coated 316L SS were 0.647 and 0.128 V, respectively. Moreover, the HAP coating on the post-passivated PoPD-coated 316L SS specimen shows an appreciable shift of E_b and E_p values towards the noble direction, 0.772 and 0.213 V, respectively. Hence a low level leach out of metal ions was observed from the HAP coating on post-passivated PoPD-coated alloy specimen when compared to the other surface-treated as well as surface-treated HAP-coated specimens as evident from ICP-AES results.

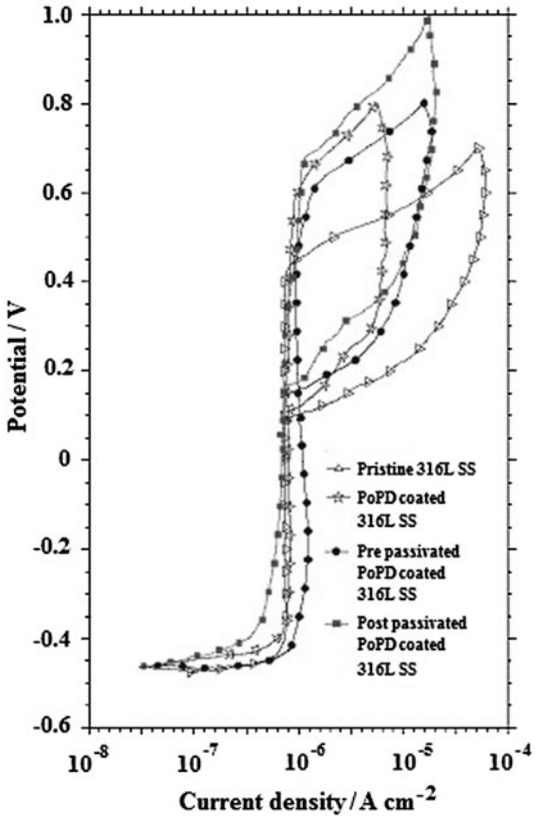

Fig. 1 Cyclic polarization curves for blank 316L SS, PoPD-coated 316L SS, the pre-passivated PoPD-coated 316L SS and the post-passivated PoPD-coated 316L SS in Ringer's solution

3.1.2 Electrochemical impedance spectra (EIS)

The EIS is a potential technique to evaluate the resistivity of the metals [33]. The impedance spectra obtained for the untreated and surface-treated and HAP-coated 316L SS specimens were fitted using equivalent circuit as shown in Fig. 3a–b.

The fitted equivalent circuit model (Fig. 3a) for the untreated 316L SS is represented as $R_s(R_{p1}C_{dl1})$, where R_s represents the solution resistance which corresponds to the ohmic resistance of the system, R_{p1} denotes the resistance to the charge transfer of the oxidation of the alloy, and C_{dl1} represents the double layer capacitance of the as-formed oxide film which is due to charge separation at metal/electrolyte interfaces. The total resistance is represented as $R_p = R_s + R_{p1}$. The spectra obtained for surface-treated as well as surface-treated HAP-coated 316L SS specimens were also fitted using the circuit model represented as $R_s(R_{p1}C_{dl1})(R_{p2}C_{dl2})$ shown in Fig. 3b, where, R_{p2} and C_{dl2} represent the resistance and capacitance of the coated system. Here the total resistance (R_p) is represented by the

Table 3 Electrochemical parameters for 316L SS under various surface treatments and coating conditions in Ringer's solution

Sample condition	Polarization parameters		Impedance parameters	
	E_b (V)	E_p (V)	R_p (Ω cm^2)	$\|Z\|$ (Ω cm^2)
Pristine 316L SS	0.453 ± 0.003	0.094 ± 0.005	42.85 ± 4.0	0.055 × 10^3 ± 0.006
PoPD-coated 316L SS	0.615 ± 0.002	0.115 ± 0.002	1560 ± 3.0	1.690 × 10^3 ± 0.004
Post-passivated PoPD-coated 316L SS	0.683 ± 0.001	0.167 ± 0.002	2822 ± 2.0	3.435 × 10^3 ± 0.003
Pre-passivated PoPD-coated 316L SS	0.620 ± 0.002	0.155 ± 0.003	1926 ± 3.0	2.065 × 10^3 ± 0.005
HAP coated on pristine 316L SS	0.488 ± 0.003	0.103 ± 0.004	854 ± 2.0	0.963 × 10^3 ± 0.004
HAP coated on PoPD-coated 316L SS	0.647 ± 0.003	0.128 ± 0.005	2270 ± 1.0	2.398 × 10^3 ± 0.002
HAP coated on post-passivated PoPD-coated 316L SS	0.772 ± 0.002	0.213 ± 0.003	3094 ± 2.0	3.775 × 10^3 ± 0.004

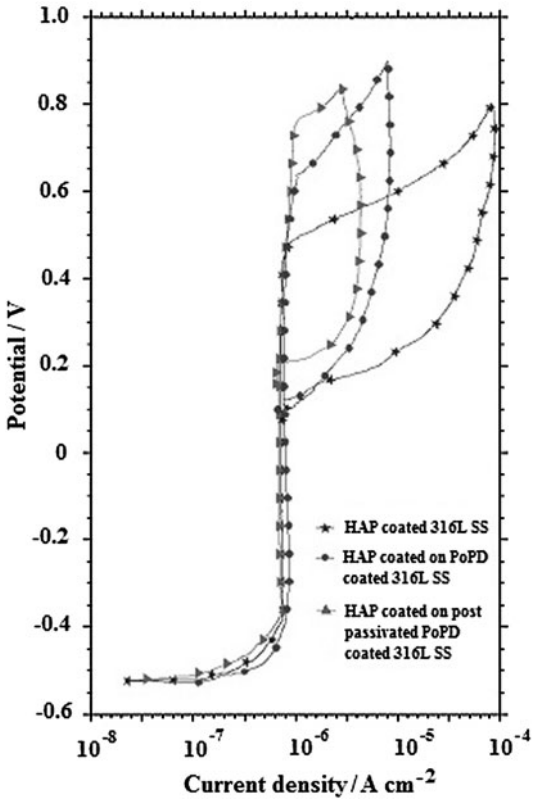

Fig. 2 Cyclic polarization curves for HAP coated on 316L SS, HAP coated on PoPD-coated 316L SS and HAP coated on the post-passivated PoPD-coated 316L SS

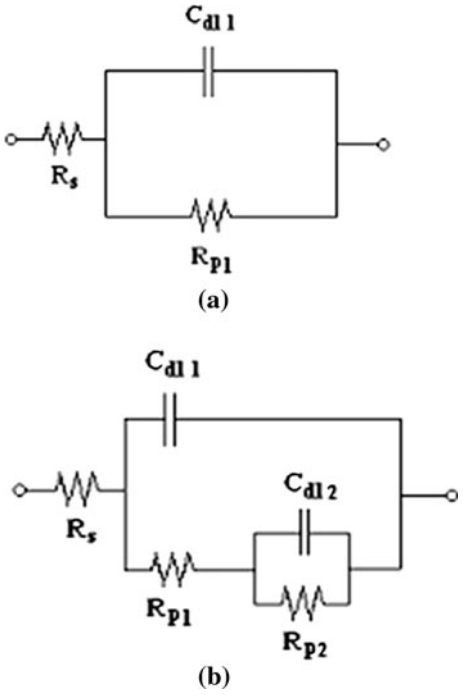

Fig. 3 Equivalent circuit diagram for **a** untreated 316L SS, **b** both the surface-treated and HAP-coated on surface-treated 316L SS specimens

sum of the resistance of the inner and outer layer, i.e., $R_P = R_s + R_{p1} + R_{p2}$.

The Nyquist and Bode plots obtained for the untreated and surface-treated 316L SS specimens in Ringer's solution at an OCP are shown in Fig. 4a, b. The impedance parameter values of untreated and surface-treated 316L SS obtained after fitting the spectra to the equivalent circuits are presented in Table 3.

The depressed semicircles obtained for the systems such as metal/passive film-PopD coating, passive film-PoPD coating/electrolyte interface can be assigned to their individual charge transfer reactions. For the uncoated 316L SS specimen, the polarization resistance and the total impedance values are 42.85 Ω and 0.055×10^3, respectively.

This may be due to the availability of the sufficient oxidative ions which paves a way for the possibility of charge transport and thereby causing the dissolution of the alloy. The 316L SS coated with PoPD showed the higher $|Z|$ and R_p values (1.690×10^3 and 1,560 Ω) due to the effective protection of SS by PoPD coating. This increase is related to the lowering of the charge transfer rate between the metal and the solution which strictly emphasize the role played by the polymer layer.

Furthermore, the calculated $|Z|$ and R_p values for the post-passivated PoPD-coated specimen were found to be 3.435×10^3 and 2,822 Ω, respectively. The significant increase observed in the $|Z|$ and R_p values suggests that an improved corrosion resistance of the alloy has occurred due to the passivation, which resulted from the stable passive oxide film developed underneath the polymer. It can be seen in Fig. 4 that the calculated $|Z|$ and R_p values obtained for the PoPD-coated SS prior to passivation were found to be 2.065×10^3 and 1,926 Ω respectively, which are much lower than that of post-passivated PoPD-coated 316L SS as discussed earlier.

Figure 5a, b shows the Nyquist and Bode plots for the HAP coated on blank 316L SS and surface-treated 316L SS specimens. The $|Z|$ and R_p values were found to be 0.963×10^3 and 854 Ω for HAP coated on the pristine 316L SS, 2.398×10^3 and 2,270 Ω for HAP coated on PoPD-coated 316L SS specimen, which then increased to 3.775×10^3 and 3,094 Ω, respectively, for HAP coated on the post-passivated PoPD-coated 316L SS specimen.

The observed increase in the $|Z|$ and R_p values is due to the highly restricted charge transfer between the alloy and the electrolyte indicating a progressive enhancement of the corrosion resistance of the coatings performed on the SS samples. The HAP layer covers the lines of the ladder conductive polymer which is well adherent to the passive film, and thus behaves as a united opponent against the penetration of corrosive ions like chloride significantly.

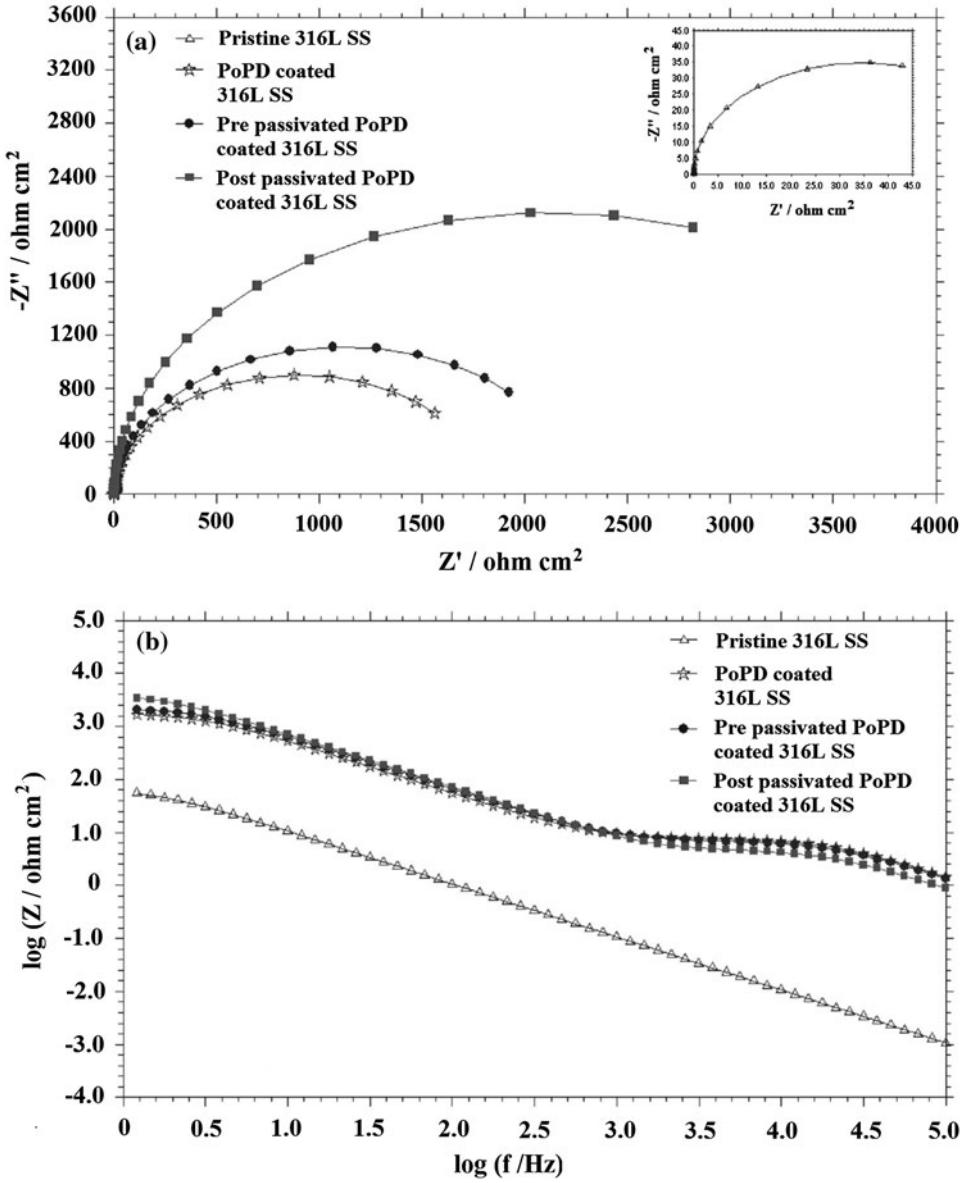

Fig. 4 Nyquist (**a**) and Bode (**b**) plots for blank 316L SS, PoPD-coated 316L SS, the pre-passivated PoPD-coated 316L SS and the post-passivated PoPD-coated 316L SS in Ringer's solution

These results are complementary to those obtained from cyclic polarization studies presented earlier. The presence of the passive film on 316L SS by borate passivation was confirmed by our previous results [19].

3.2 Cyclic voltammetry

Figure 6 shows the cyclic voltammetric curves for the PoPD-coated 316L SS at three different CV cycles followed by the borate passivation at 0.64 V. Briefly, in all the three cases the first anodic peak at potential −0.4 V can be ascribed to the oxidation of Fe(II) to Fe(III), i.e., (Fe_2O_3). The oxidation of Cr(III)-oxide to soluble Cr(VI) species occurred at a potential of 0.63 V is most likely to be $Cr_2O_7^{2-}$. In the reduction cycle, two peaks at 0 V and 0.57 V are ascribed to the reduction of Cr(VI) to Cr(III) occurring in the oxide film and reduction of Fe(III) composed of Fe_2O_3 back to Fe(II) species, respectively [12, 19]. This confirms the protective nature of the passive film formed underneath the PoPD. The current density of cathodic and anodic peaks increases linearly with increasing CV cycles for PoPD deposition. Thus, the PoPD coating done at 50 cycles was fixed as an optimum for getting better passivation. The cyclic voltammetric curves for the pre and post-passivated PoPD-coated SS is shown in Fig. 7. In the passivation of SS through PoPD coating, the values of current density of cathodic and anodic peaks for chromium ion are found to be drastically higher than the pre-passivated SS, thus confirming the formation of Cr-enriched passive film. This observation leads to the conclusion that, selective dissolution of Fe by the PoPD occurs, leaving chromium-enriched passive film

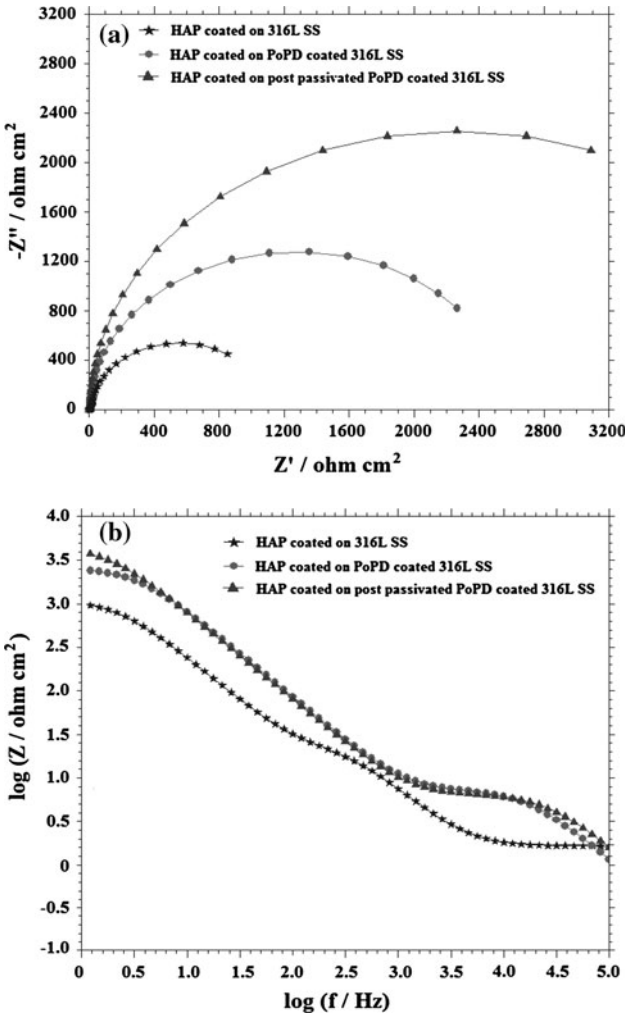

Fig. 5 Nyquist (**a**) and Bode (**b**) plots for HAP coated on 316L SS, HAP coated on the PoPD-coated 316L SS and HAP coated on the post-passivated PoPD-coated 316L SS

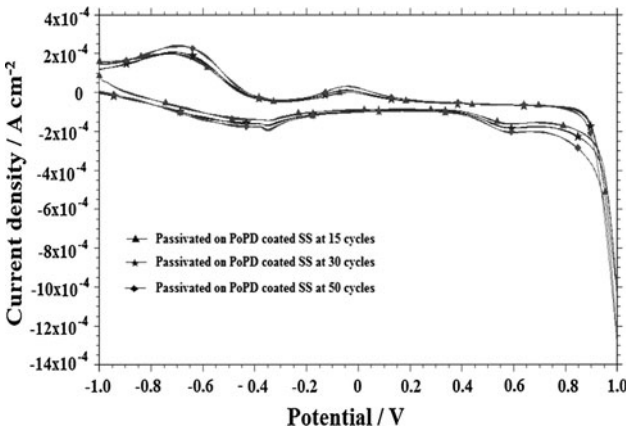

Fig. 6 Cyclic voltammetric curves for the PoPD-coated 316L SS at three different cycles followed by passivation in borate buffer solution

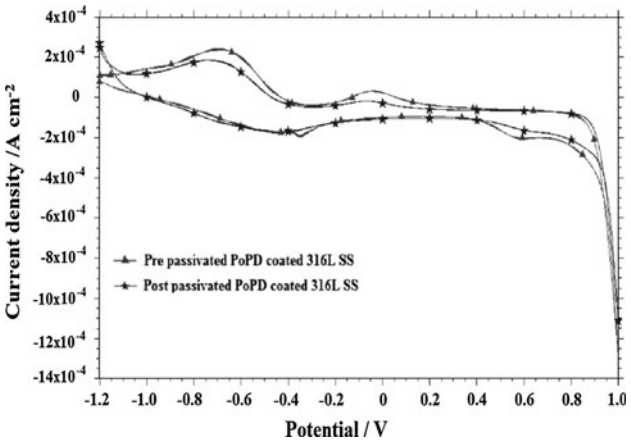

Fig. 7 Cyclic voltammetric curves for the post-passivated PoPD-coated 316L SS and the pre-passivated PoPD-coated 316L SS in borate buffer solution

[29, 30]. This indicates that the passivation of SS through the PoPD coating significantly contributes to the enhancement of the passive properties of the surface oxide film. This passive film prevents the dissolution of the underlying metal alloy into the solution even at higher anodic potentials.

3.3 Surface characterization studies

3.3.1 XRD studies

The XRD results for the borate passivation followed by the PoPD coating on the SS (Fig. 8a) show the peaks for iron oxide (Fe_2O_3) (JCPDS: 33-664), chromium oxide (Cr_2O_3) (JCPDS: 38-1479) and a few for the substrate (316L SS) as well. However, in the case of the PoPD coated followed by the borate passivated on SS, the peaks for chromium oxide exhibit an appreciable increase in intensity with respect to the pre-passivated PoPD-coated SS as depicted in Fig. 8b. This confirms the selective dissolution of iron and the chromium enrichment in the passive film underneath the polymer.

3.3.2 X-ray photoelectron spectroscopy studies

To further substantiate the above discussions, the X-ray photoelectron spectroscopy (XPS) measurements are used to directly characterize and confirm the composition of passive film formed on SS specimens at two different surface treatment conditions. The XPS survey spectra for the pre-passivated PoPD-coated 316L SS and post-passivated PoPD-coated 316L SS are shown in Fig. 9a, b. In these survey spectra, the whole range of binding energies were analyzed and found that the passive film is composed of the following elements such as iron (700–740 eV), chromium (570–582 eV), oxygen (520–540 eV), and carbon (282–291 eV) in the form of oxides of chromium and

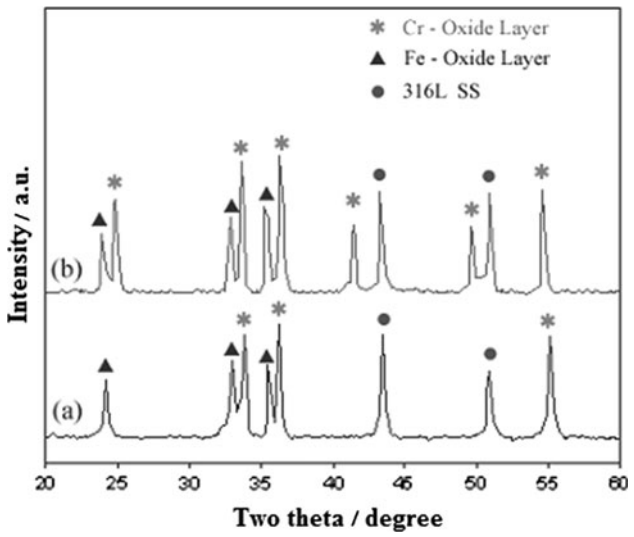

Fig. 8 XRD pattern of (*a*) pre-passivated PoPD-coated 316L SS and (*b*) post-passivated PoPD-coated 316L SS

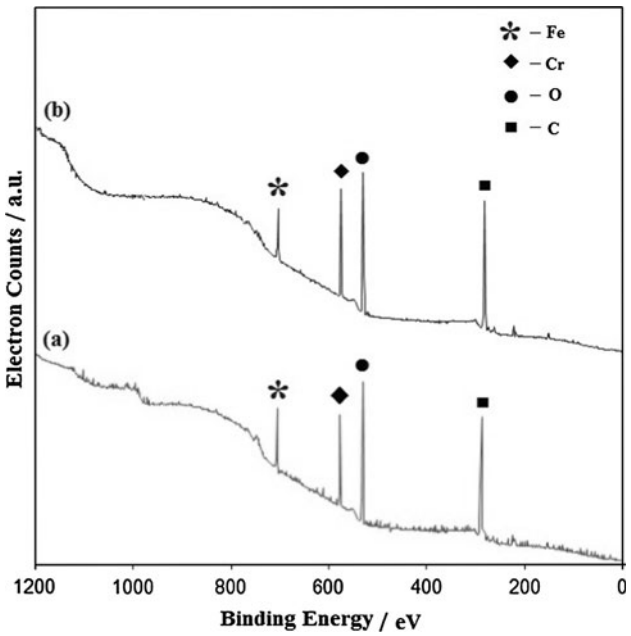

Fig. 9 XPS survey spectra for (*a*) pre-passivated PoPD-coated 316L SS and (*b*) post-passivated PoPD-coated 316L SS

iron (Fig. 9a, b) [33, 34]. Several authors have shown that the passive film on SS exhibits a duplex character with an inner chromium oxide-enriched part and an outer iron oxide-enriched part where the protective character of the passive film is mainly attributed to the inner part [34–40].

Interestingly, for the post-passivated PoPD-coated 316L SS (Fig. 9b), the oxygen and chromium levels are found to be higher when compared to the pre-passivated PoPD-coated 316L SS sample (Fig. 9a) which strongly evidence the enrichment of chromium ion in the as-formed passive film underneath the polymer. Consolidating the XPS survey spectra results, one may state that the passivation of 316L SS through the PoPD coating (post-passivation) led to the chromium-enriched passive oxide film underneath the polymer which makes the system highly bioresistive.

3.4 Scanning electron microscopic investigations

Figure 10 shows the scanning electron microscopic (SEM) images of pristine, surface-treated, and surface-treated HAP-coated 316L SS specimens in Ringer's solution at an impressed potential for 1 h. The pristine 316L SS specimen placed in Ringer's solution (Fig. 10a) shows the formation of pits due to the dissolution of metal ions from this sample as there is no protective film over its surface [41]. A transparent and compact polymer layer formed after 50 cycles is shown in Fig. 10b. The morphology of PoPD layer on SS consists of a net of broad lines and reflects light. These lines are similar to the conductive lines appeared in the transparent films of ladder CPs [30, 42]. It is also observed from the SEM images that, the growth of pits has almost stopped in 316L SS specimens containing the polymer layer (Fig. 10b) and HAP coating over the polymer layer (Fig. 10c). Further, the SEM image of the uniform HAP coating (Fig. 10d) obtained over the post-passivated PoPD-coated SS shows no pits, thus proving the improved corrosion resistance behavior of 316L SS in Ringer's solution.

The cross-sectional SEM morphological observations of the HAP coating on the post-passivated PoPD-coated 316L SS with low and high magnifications are shown in Fig. 11a, b. From the low magnification image (Fig. 11a), it could be observed that the particles in both PoPD and HAP layers are well tightly bonded to each other. Moreover, the coatings formed are found to be smooth and uniform without delamination and/or cracks at the interface as portrayed in SEM. The presence of passive film underneath the polymer layer was also observed by the higher resolution SEM image as shown in Fig. 11b, and the thickness of the passive film was found to be about $\sim$18 nm. Therefore, the results obtained from the electrochemical and surface characterization techniques were substantiated by SEM cross-sectional study that the enhanced corrosion resistivity of the HAP coating on post-passivated PoPD-coated 316L SS surface is attributed to the protective primary passive film underneath the PoPD/HAP coating.

3.5 Adhesion results

Adhesion of the coatings to the substrate is of the utmost importance for an implant to function properly in physiological conditions. Failure of the implant takes place when decohesion of the coating occurs. Figure 12 represents the adhesion strength of various types of coatings on 316L SS,

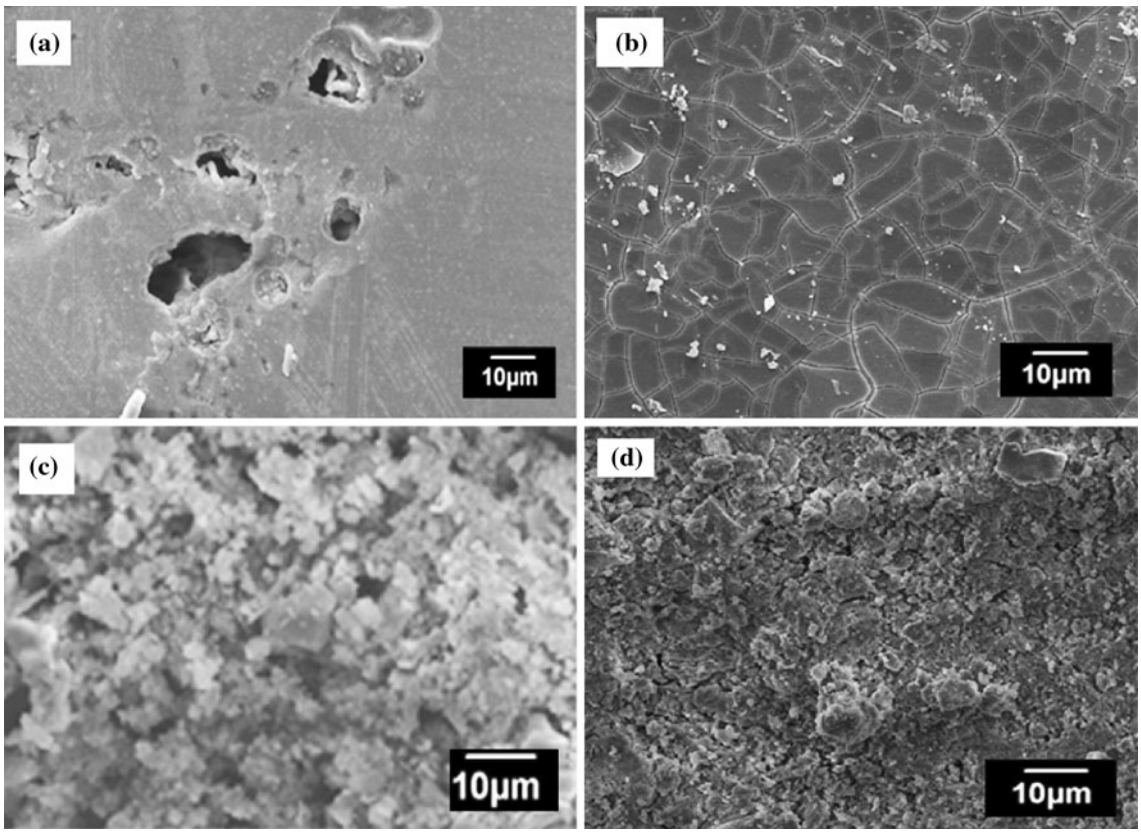

Fig. 10 SEM image of **a** pristine 316L SS, **b** PoPD-coated 316L SS, **c** HAP coated on the PoPD coated 316L SS, and **d** HAP coated on the post-passivated PoPD-coated 316L SS, in Ringer's solution

and it is evident that the measured adhesive strength for the HAP coating on pristine 316L SS was found to be 11.8 ± 0.7 MPa. Whereas in the case of HAP coating on the post-passivated PoPD-coated 316L SS, the measurement of adhesive strength is considered as two systems, i.e., (i) the adhesion strength of passive film combined with PoPD coating on the 316L SS substrate is 16.5 ± 0.6 MPa; (ii) the adhesion strength between the PoPD layer and the HAP coating is 14.4 ± 0.6 MPa. The adhesion strength of the passive film/PoPD coating on 316L SS was found to be higher which could be due to the intactness of the PoPD layer with the homogeneous rough thin passive film formed on the 316L SS (as discussed earlier in SEM cross-sectional image shown in Fig. 11b). This increased adhesion strength may also due to the electron transfer reactions during the formation of PoPD coating on 316L SS. So the chemical bond appears between the PoPD coating and the substrate may be an ionic bond. Further, the HAP coating on the ladder conductive polymer PoPD is so compact and facilitated a better adhesion strength while compared to that of the HAP coating on the pristine 316L SS. Hence the passivation of 316L SS through the PoPD coating improves the adhesion strength of the whole system.

3.6 Leach out analysis

An accelerated leaching out characteristics of the specimen in Ringer's solution after aging of 1 h at an impressed potential of 0.46 V was performed by ICP-AES analysis and is portrayed in Fig. 13. A significant amount of metal ions namely Fe, Cr, Ni, and Mo were leached out from the pristine 316L SS without any surface treatment. This is attributed to the fact that there is no barrier film on the alloy surface to prevent the attack of chloride ions. When the SS specimen was subjected to the PoPD coating followed by a borate passivation, the leach out of metal ions was found to be lower than that of the pre-passivated one. This observation leads to the confirmation that the as-formed, chromium-enriched passive oxide film by the PoPD in its underneath protects the alloy surface and reduces the rate of the metal ion dissolution. Thus, the PoPD layer plays a dual role of forming the chromium-enriched passive oxide film in its underneath (Fig. 14) as well as to protect the breakdown of passive film from the harsh environment in our body which in turn offers an enhanced corrosion protection of implant material with longer life time.

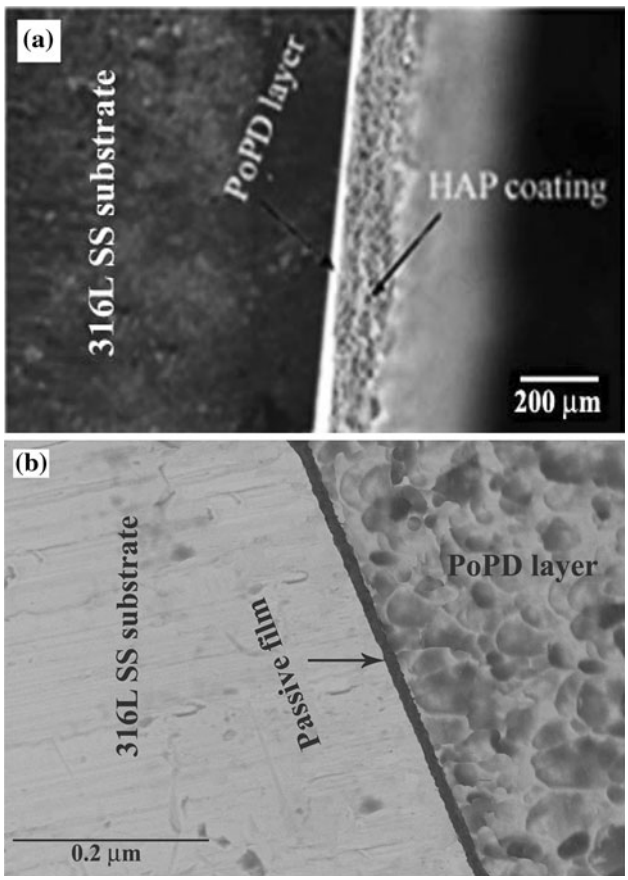

Fig. 11 SEM cross-sectional micrographs of HAP coating on the post-passivated PoPD-coated 316L SS in Ringer's solution. **a** *Low* magnification, **b** *high* magnification for the detection of passive film

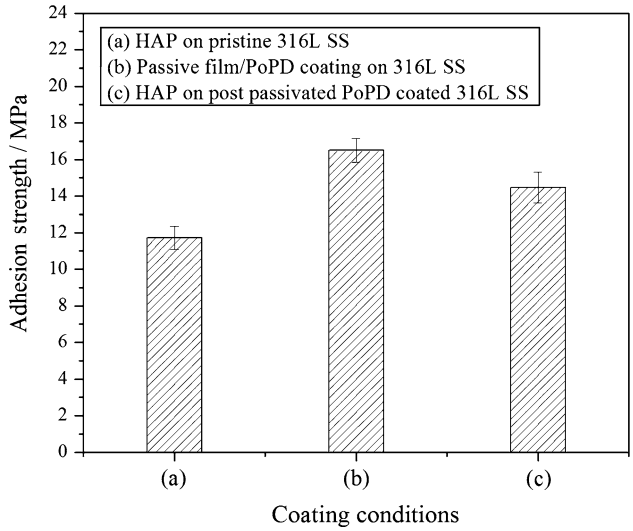

Fig. 12 Adhesion strength of the different coating

Furthermore, in the case of HAP coating on the post-passivated PoPD-coated SS specimen, the dissolution tendency of metal ions are considerably reduced at the impressed potential (0.46 V) than other surface-treated SS

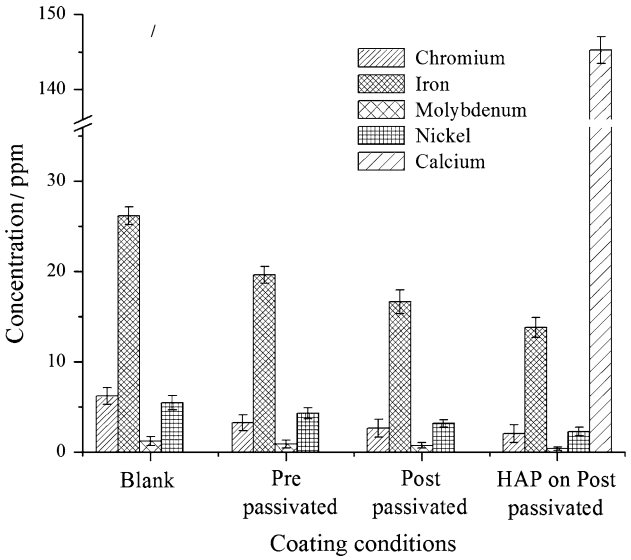

Fig. 13 Leach out characteristics of different coating condition on 316L SS in Ringer's solution

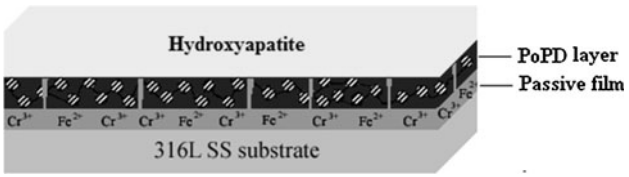

Fig. 14 An illustrative schematic representation of the trilayer formed on 316L SS

specimens. However, the dissolution of Ca could not be prevented from the coating at this impressed potential. Thus, the coating of PoPD followed by a borate passivation in 316L SS can certainly decrease the release of metallic ions and their deleterious effects. Hence, this approach can be regarded as a potential passivation method that can be used prior to the development of biocompatible HAP coating over the biomedical implants. So, it is possible to assume that these coatings (Fig. 14) represent good resistance to metal ions leach out when implanted into real systems.

3.7 Hardness results

The Vicker's microhardness (H_v) values for the PoPD-coated 316L SS, the post-passivated PoPD-coated 316L SS and HAP coated on the post-passivated PoPD-coated 316L SS specimens are shown in Fig. 15. For the PoPD-coated 316L SS and the post-passivated PoPD-coated 316L SS specimens the Vicker's microhardness values were found to be 400.00 ± 15.81 and 410 ± 11.35, respectively. The H_v value of 435.32 ± 13.42 is obtained for the HAP coatings on the post-passivated PoPD-coated 316L SS

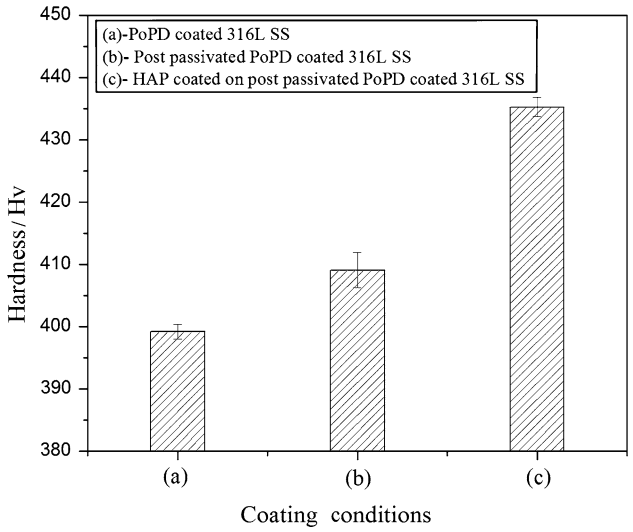

Fig. 15 The Vicker's microhardness graph of the PoPD-coated 316L SS, post-passivated PoPD-coated 316L SS and HAP on post-passivated PoPD-coated 316L SS

which is higher than that of the surface-treated 316L SS specimens.

3.8 The biocompatibility test

In order to assess the biocompatibility of the post-passivated PoPD-coated 316L SS, the specimen was immersed in SBF for various numbers of days. Figure 16 shows the FT-IR spectra of the bioactive layer formed on the surface of the post-passivated PoPD-coated 316L SS specimen when

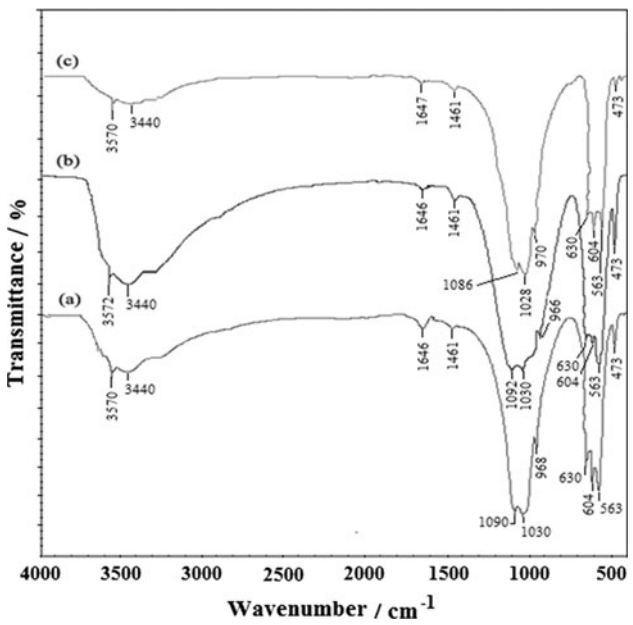

Fig. 16 FTIR spectra of bioactive layer on the surface of the post-passivated PoPD-coated 316L SS specimen after immersion in SBF for (*a*) 7 days, (*b*) 14 days, and (*c*) 21 days

immersed in SBF solution for various numbers of days. In all the cases, the peaks are attributed to calcium phosphate apatite. For the specimen with 7 days in SBF (Fig. 16a), the two asymmetric P–O stretching (υ_3) peaks were found at 1,090 and 1,030 cm^{-1}. One asymmetric P–O stretching (υ_1) peak was found at 968 cm^{-1} and two asymmetric O–P–O bending (υ_4) peaks were detected at 604 and 563 cm^{-1}, respectively. Also, a symmetrical O–P–O bending (υ_2) peak is present at 473 cm^{-1}. The molecular and adsorbed water bands are observed at 1,646 and 3,440 cm^{-1}. The stretching and bending vibrational modes for phosphates were observed at 3,570 and 630 cm^{-1} [43].

On increasing the soaking time to 14 days (Fig. 16b), the above peak positions are retained. For instance, the characteristic phosphate peaks were found at 473, 563, 604, 966, 1030, and 1,092 cm^{-1}. The hydroxyl stretching and bending vibrations are observed at 3,572 cm^{-1} and 630 cm^{-1}. The existence of adsorbed water is found at 3,440 and 1,646 cm^{-1}. As can be seen in Fig. 16c, it is evident that on further increasing the soaking time to 21 days, the below said calcium phosphate peaks for apatite formation is observed. The υ_1 and υ_3 phosphate modes are observed at 970 and 1028, 1086 cm^{-1}. The peaks at 473, 563, and 604 cm^{-1} are attributed to υ_2 and υ_4 phosphate mode. The absorbance of lattice water is also sensed at 3,440 and at 1,647 cm^{-1}. A significant concentration of hydroxyl groups remains in the structure as evident from the intensity of stretching and bending vibration peaks found at 3,570 and 630 cm^{-1}, respectively. Besides, a more detailed analysis permits one to deduce the presence of a carbonated component in all the cases, which have been detected at 1,461 cm^{-1}. Hence the appearance of phosphate and carbonate absorption bands in the spectra of post-passivated PoPD-coated 316L SS sample after immersion in SBF for various days confirms the formation of calcium phosphate apatite layer on their surface. The formation of apatite layer on the surface of the post-passivated PoPD-coated 316L SS after soaking in SBF for various days was ascertained by SEM micrographs shown in Fig. 17a–c. It can be seen in from Fig. 17a that a new apatite layer with spherical particle that formed after 7 days of immersion in SBF, completely covers the surface of the sample as shown. The HAP growth was observed over the entire surface and with the increasing time, i.e., after 14 days, the new apatite layer becomes smooth, more compact and uniform as seen in Fig. 17b indicating the presence of greater bioactivity and biocompatibility of the sample.

A further increase of soaking time to 21 days, as shown in Fig. 17c, has no influence on the morphology of the newly grown apatite layer except an increase in the thickness suggesting an increased bioactivity of the sample. The agglomeration of apatite particles is also evident from

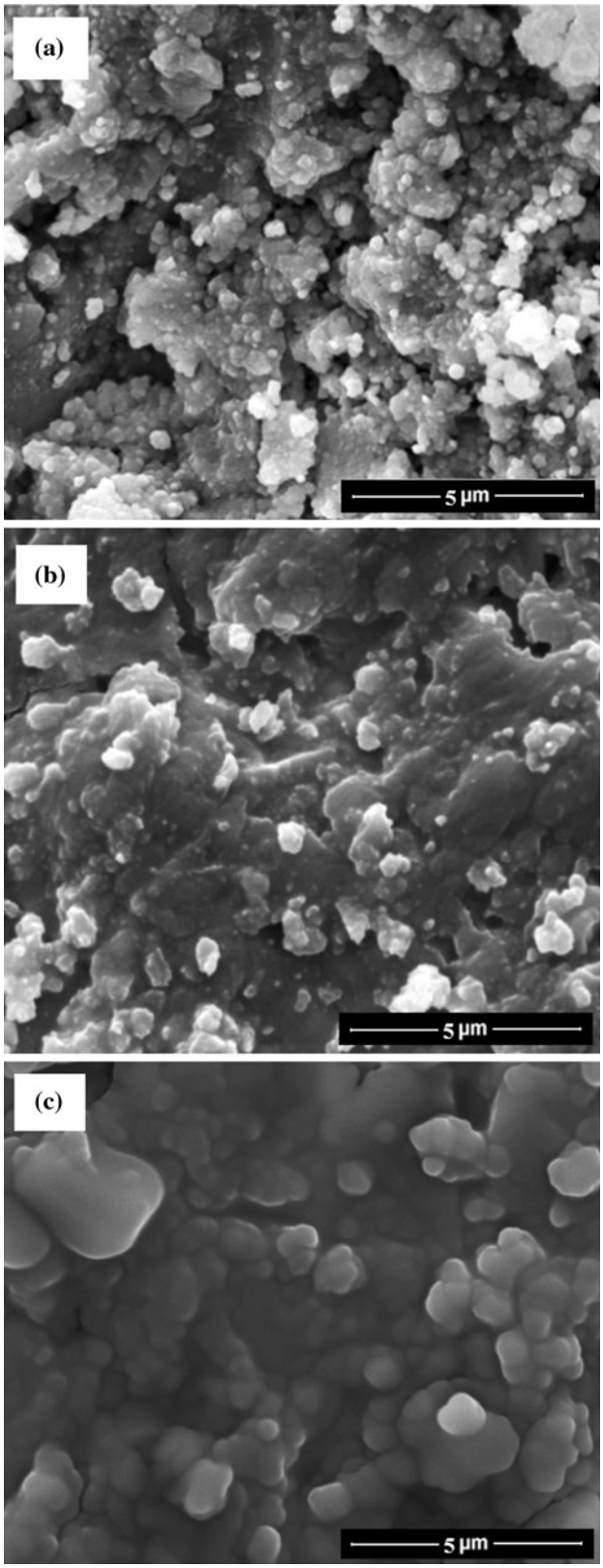

Fig. 17 SEM images of the post-passivated PoPD-coated 316L SS specimen after immersion in SBF for **a** 7 days, **b** 14 days, and **c** 21 days

the SEM image on increasing the soaking time in SBF. Therefore, the SEM results substantiate the formation of apatite layer on the surface of the post-passivated PoPD-coated 316L SS. Hence, the surface treatment of 316L SS in terms of the PoPD coating followed by a borate passivation could be a better bioactive and biocompatible material which was confirmed by both FT-IR and SEM results.

4 Conclusions

The HAP coating on the post-passivated PoPD-coated 316L SS was found to have an impact on improving the corrosion resistance as evidenced from the complementary polarization and EIS results. The chromium-enriched passive film formed underneath the PoPD layer was confirmed by cyclic voltammetric technique showing an anodic peak at 0.63 V and cathodic peak at 0 V with an increased current density and also evidenced from XRD and XPS results. The PoPD coating on 316L SS plays a dual role, i.e., it selectively passivates the SS in its underneath as well as sensitively protecting the as-formed passive film. The scanning electron microscopic results obtained for HAP coating on the post-passivated PoPD-coated 316L SS show no pit formation, thus confirming the enhanced corrosion resistivity of the coatings and this was further substantiated by ICP-AES results, indicating the lowest leach out of metal ions. The increased hardness value for the HAP coated on PoPD-coated 316L SS was due to the formation of dense structure and low porosity coatings. The in vitro test for the post-passivated PoPD-coated 316L SS in SBF induced the apatite formation thus confirming the increased bioactivity of the specimen. On the basis of the above observations, it is concluded that the HAP coating on the post-passivated PoPD-coated 316L SS material is biocompatible, possesses an excellent corrosion resistance, and hence act as a promising implant material for biomedical applications.

Acknowledgments One of the authors D. Gopi acknowledges the major financial support from the Indian Council of Medical Research (ICMR, IRIS ID No. 2010-08660, Ref. No: 5/20/11(Bio)/10-NCD-I), Department of Science and Technology (DST-SERC, Ref. No: SR/FTP/ETA-04/2009 and DST-TSD, Ref. No.: DST/TSG/NTS/2011/73) and Council of Scientific and Industrial Research (CSIR, Ref. No.: 01(2547)/11/EMR-II), New Delhi, India in the form of major research projects. Another author (J. Indira) wishes to thank the Council of Scientific and Industrial Research (CSIR), New Delhi, India for the award of Senior Research Fellowship (CSIR-SRF). L. Kavitha acknowledges the financial support from International Centre for Theoretical Physics (ICTP), Italy in the form of Junior Associateship. The support from CICECO, University of Aveiro, Portugal is also acknowledged.

References

1. Garcia C, Cere S, Duran A (2004) Bioactive coatings prepared by sol–gel on stainless steel 316L. J Non-Cryst Solids 348:218–224. doi:10.1016/j.jnoncrysol.2004.08.172
2. Meinert K, Uerpmann C, Matschullat J, Wolf GK (1998) Corrosion and leaching of silver doped ceramic IBAD coatings on SS 316L under simulated physiological conditions. Surf Coat Technol 58:103–104
3. Nagarajan S, Rajendran N (2009) Surface characterisation and electrochemical behaviour of porous titanium dioxide coated 316L stainless steel for orthopaedic applications. App Surf Sci 255:3927–3932. doi:10.1016/j.apsusc.2008.10.058
4. Ballarre J, Lopez DA, Schreiner WH, Duran A, Cere SM (2007) Protective hybrid sol–gel coatings containing bioactive particles on surgical grade stainless steel: surface characterization. Appl Surf Sci 253:7260–7264. doi:10.1016/j.apsusc.2007.03.007
5. Okazaki Y, Gotoh E, Manabe T, Kobayashi K (2004) Comparison of metal concentrations in rat tibia tissues with various metallic implants. Biomaterials 25:5913–5920. doi:10.1016/j.biomaterials.2004.01.064
6. Woodman JL, Black J, Nunamaker DM (1983) Release of cobalt and nickel from a new total finger joint prosthesis made of vitallium. J Biomed Mater Res 17:655–668. doi:10.1002/jbm.820170410
7. Gurappa I (2002) Development of appropriate thickness ceramic coatings on 316 L stainless steel for biomedical applications. Surf Coat Technol 161:70–78
8. Bordjih K, Jouzeau JY, Mainard D, Payan E, Delagoutte JP (1996) Evaluation of the effect of three surface treatments on the biocompatibility of 316L stainless steel using human differentiated cells. Biomaterials 17:491–500
9. Sivakumar M, Rajeswari S (1992) Investigation of failures in stainless steel orthopaedic implant devices: pit-induced stress corrosion cracking. J Mater Sci Lett 11:1039–1042. doi:10.1007/BF00729754
10. Sridhar TM, Arumugam TK, Rajeswari S, Subbaiyan M (1997) Electrochemical behaviour of hydroxyapatite-coated stainless steel implants. J Mater Sci Lett 16:1964–1966. doi:10.1023/A:1018511406374
11. Shibli SMA, Jayalekshmi AC (2008) Development of phosphate inter layered hydroxyapatite coating for stainless steel implants. Appl Surf Sci 254:4103–4110. doi:10.1016/j.apsusc.2007.12.051
12. Kocijan A, Donik C, Jenko M (2006) Electrochemical and XPS studies of the passive film formed on stainless steel in borate buffer and chloride solutions. Corros Sci 49:2083–2098. doi:10.1016/j.corsci.2006.11.001
13. Prabakaran K, Rajeswari S (2009) Electrochemical, SEM and XPS investigations on phosphoric acid treated surgical grade type 316L SS for biomedical applications. J Appl Electrochem 39:887–897
14. Nazneen F, Galvin P, Arrigan DWM, Thompson M, Benvenuto P, Herzog G (2011) Electropolishing of medical-grade stainless steel in preparation for surface nano-texturing. J Solid State Electrochem 16:1389–1397. doi:10.1007/s10008-011-1539-9
15. Flis J, Wydorska MK, Kabulska IF (2006) The effect of molybdenum on corrosion of low-temperature nitrided stainless steels in sulphate-chloride solution. J Solid State Electrochem 10:689–695. doi:10.1007/s10008-006-0112-4
16. Hong T, Ogushi T, Nagumo M (1996) The effect of chromium enrichment in the film formed by surface treatments on the corrosion resistance of type 430 stainless steel. Corros Sci 38:881–888. doi:10.1016/0010-938X(96)00174-6
17. Noh JS, Laycock NJ, Gao W, Wells DB (2000) Effects of nitric acid passivation on the pitting resistance of 316 stainless steel. Corros Sci 42:2069–2084. doi:10.1016/S0010-938X(00)00052-4
18. Shih CC, Shih CM, Su YY, Su LHJ, Chang MS, Lin SJ (2004) Effect of surface oxide properties on corrosion resistance of 316L stainless steel for biomedical applications. Corros Sci 46:427–441. doi:10.1016/S0010-938X(03)00148-3
19. Gopi D, Collins Arun Prakash V, Kavitha L (2009) Evaluation of hydroxyapatite coatings on borate passivated 316L SS in Ringer's solution. Mater Sci Eng C 29:955–958. doi:10.1016/j.msec.2008.08.020
20. O'Neill RD, Lowry JP, Rocchitta G, McMahon CP, Serra PA (2008) Designing sensitive and selective polymer/enzyme composite biosensors for brain monitoring in vivo. Trends Anal Chem 27:78–88. doi:10.1016/j.trac.2007.11.008
21. Dixon BM, Lowry JP, O'Neill RD (2002) Characterization in vitro and in vivo of the oxygen dependence of an enzyme/polymer biosensor for monitoring brain glucose. J Neurosci Methods 119:135–142. doi:10.1016/S0165-0270(02)00170-X
22. Killoran SJ, O'Neill RD (2008) Characterization of permselective coatings electrosynthesized on Pt–Ir from the three phenylenediamine isomers for biosensor applications. Electrochim Acta 53:7303–7312. doi:10.1016/j.electacta.2008.03.076
23. McMahon CP, Killoran SJ, O'Neill RD (2005) Design variations of a polymer-enzyme composite biosensor for glucose: enhanced analyte sensitivity without increased oxygen dependence. J Electroanal Chem 580:193–202. doi:10.1016/j.jelechem.2005.03.026
25. O'Neill RD, Lowry JP, Mas M (1998) Monitoring brain chemistry in vivo: voltammetric techniques, sensors, and behavioral applications. Crit Rev Neurobiol 12:69–127. doi:10.1615/CritRevNeurobiol.v12.i1-2.40
26. Kirwan SM, Rocchitta G, McMahon CP, Craig JD, Killoran SJ, O'Brien KB, Serra PA, Lowry JP, O'Neill RD (2007) Modifications of poly(*o*-phenylenediamine) permselective layer on Pt–Ir for biosensor application in neurochemical monitoring. Sensors 7:420–437. doi:10.3390/s7040420
27. Killoran SJ, Rai DK, O'Neill RD (2007) Comparison of phenylenediamine isomers for the synthesis of permselective biosensor polymers for neurochemical analysis. J Neuro Chem 102:196–197
28. O'Neill RD, Lowry JP (1995) On the significance of brain extracellular uric acid detected with in vivo monitoring techniques: a review. Behav Brain Res 71:33–49. doi:10.1016/0166-4328(95)00035-6
29. Hermas AA (2008) XPS analysis of the passive film formed on austenitic stainless steel coated with conductive polymer. Corros Sci 50:2498–2505. doi:10.1016/j.corsci.2008.06.019
30. Hermas AA (2008) Protection of type 430 stainless steel against pitting corrosion by ladder conductive polymer. Prog Org Coat 61:95–102. doi:10.1016/j.porgcoat.2007.09.005
31. Gopi D, Indira J, Collins Arun Prakash V, Kavitha L (2009) Spectroscopic characterization of porous nanohydroxyapatite synthesized by a novel amino acid soft solution freezing method. Spectrochim Acta A 74:282–284. doi:10.1016/j.saa.2009.05.021
32. Kokubo T, Takadama H (2006) How useful is SBF in predicting in vivo bone bioactivity? Biomaterials 27:2907–2915. doi:10.1016/j.biomaterials.2006.01.017
33. Cano E, Lafuente D, Bastidas DM (2010) Use of EIS for the evaluation of the protective properties of coatings for metallic cultural heritage: a review. J Solid State Electrochem 14:381–391. doi:10.1007/s10008-009-0902-6
34. Milosev I, Strehblow HH (2000) The behavior of stainless steels in physiological solution containing complexing agent studied by X-ray photoelectron spectroscopy. J Biomed Res 52:404–412. doi:10.1007/s10856-006-0180-0
35. Hryniewicz T, Rokosz K, Rokicki R (2008) Electrochemical and XPS studies of AISI 316L stainless steel after electropolishing in a magnetic field. Corros Sci 50:2676–2681. doi:10.1016/j.corsci.2008.06.048

36. Ramasubramanian N, Preocanin N, Davidson RD (1985) Analysis of passive films on stainless steel by cyclic voltammetry and auger spectroscopy. J Electrochem Soc 132:793–798. doi:10.1149/1.2113959
37. Hakiki NE, Belo MDC, Simoes AMP, Ferreira MGS (1998) Semiconducting properties of passive films formed on stainless steels: influence of the alloying elements Electrochemical Science and Technology. J Electrochem Soc 145:3821–3829. doi:10.1149/1.1838880
38. Olefjord I, Bronx B, Jelvestam U (1985) Surface composition of stainless steels during anodic dissolution and passivation studied by ESCA. J Electrochem Soc 132:2854–2861. doi:10.1149/1.2113683
39. Calinski C, Strehblow HH (1989) ISS depth profiles of the passive layer on Fe/Cr alloys. J Electrochem Soc 136:1328–1331. doi:10.1149/1.2096915
40. Lorang G, Belo MDC, Simoes AMP, Ferreira MGS (1994) Chemical composition of passive films on AISI 304 stainless steel. J Electrochem Soc 141:3347–3356. doi:10.1149/1.2059338
41. Wang W, Zhang X, Wang J (2009) Pits with coloured halos formed on 1Cr–18Ni–9Ti stainless steel surface after ennoblement in seawater. Mater Sci Eng C 29:851–855. doi:10.1016/j.msec.2008.07.034
42. Belaish I, Davidov D, Selig H, McLean MR, Dalton L (1989) Spatially selective conducting patterns in transparent films derived from ladder type polymers. Angew Chem Int Ed Engl Adv Mater 28:1569–1571. doi:10.1002/anie.198915691
43. Tamilselvi S, Raman V, Rajendran N (2010) Evaluation of corrosion behavior of surface modified Ti–6Al–4V ELI alloy in hanks solution. J Appl Electrochem 40:285–293. doi:10.1007/s10800-009-9972-5